JACS
JOURNAL OF THE AMERICAN CHEMICAL SOCIETY
pubs.acs.org/JACS
Article

All-Solid-State Lithium–Sulfur Batteries Enhanced by Redox Mediators

Xin Gao, Xueli Zheng, Yuchi Tsao, Pu Zhang, Xin Xiao, Yusheng Ye, Jun Li, Yufei Yang, Rong Xu, Zhenan Bao, and Yi Cui*

Cite This: J. Am. Chem. Soc. 2021, 143, 18188–18195
Read Online
ACCESS | Metrics & More | Article Recommendations | Supporting Information

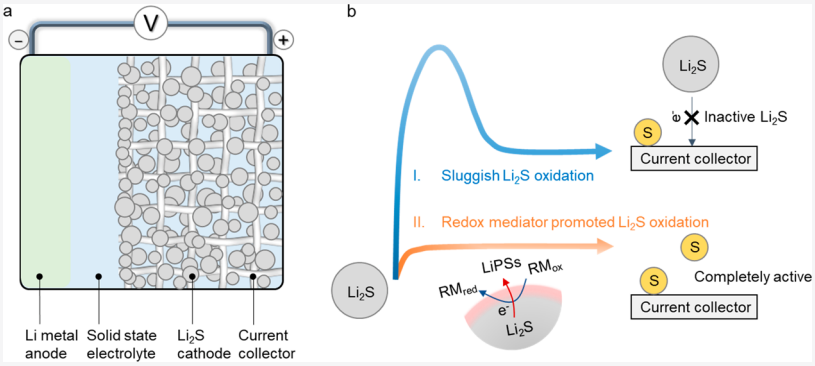

ABSTRACT: Redox mediators (RMs) play a vital role in some liquid electrolyte-based electrochemical energy storage systems. However, the concept of redox mediator in solid-state batteries remains unexplored. Here, we selected a group of RM candidates and investigated their behaviors and roles in all-solid-state lithium–sulfur batteries (ASSLSBs). The soluble-type quinone-based RM (AQT) shows the most favorable redox potential and the best redox reversibility that functions well for lithium sulfide (Li_2S) oxidation in solid polymer electrolytes. Accordingly, Li_2S cathodes with AQT RMs present a significantly reduced energy barrier (average oxidation potential of 2.4 V) during initial charging at 0.1 C at 60 °C and the following discharge capacity of 1133 mAh g_s^{-1}. Using *operando* sulfur K-edge X-ray absorption spectroscopy, we directly tracked the sulfur speciation in ASSLSBs and proved that the solid–polysulfide–solid reaction of Li_2S cathodes with RMs facilitated Li_2S oxidation. In contrast, for bare Li_2S cathodes, the solid–solid Li_2S–sulfur direct conversion in the first charge cycle results in a high energy barrier for activation (charge to ~4 V) and low sulfur utilization. The Li_2S@AQT cell demonstrates superior cycling stability (average Coulombic efficiency 98.9% for 150 cycles) and rate capability owing to the effective AQT-enhanced Li–S reaction kinetics. This work reveals the evolution of sulfur species in ASSLSBs and realizes the fast Li–S reaction kinetics by designing an effective sulfur speciation pathway.

INTRODUCTION

Redox mediators (RMs) that are reversibly oxidized and reduced upon electrochemical cycling play an important role in achieving satisfactory performance for many electrochemical energy storage systems.[1] In the area of lithium-ion batteries, RMs induce the reversible oxidation/reduction at a slightly higher oxidation potential than the fully charged voltage to release extra charge, which works as chemical overcharge protection agents in the liquid electrolyte to improve the safety of batteries.[2−4] For next-generation batteries such as lithium–oxygen and lithium–sulfur batteries,[5] RMs are incorporated as liquid electrolyte additives to promote charge transfer at the electrode–electrolyte interface, thus activating insulating discharged products such as lithium oxide/lithium peroxide[6−8] and sulfur/lithium sulfide (Li_2S).[9−11] So far, the studies of RMs have been focused on liquid electrolytes. It is unknown whether the RM concept can also be applied to the solid-state system since the solubility and diffusivity of RMs in a solid-state system is very limited.

All-solid-state lithium–sulfur batteries (ASSLSBs) have received enormous attention owing to their high specific capacity (1675 mAh g^{-1}), high safety, and low cost.[12−14] Extensive efforts have been made to seek desired solid-state electrolytes for the satisfactory battery performance.[15,16] In particular, solid polymer electrolytes (SPEs), mixtures of solid polymers and lithium salts, hold great promise owing to their better thermal stability than conventional liquid electrolytes

Received: July 25, 2021
Published: October 22, 2021

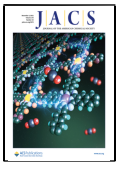

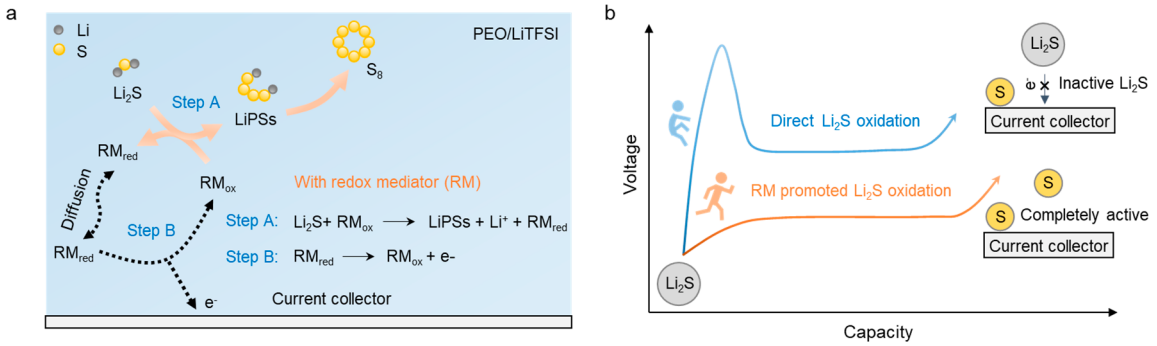

Figure 1. Role of redox mediators (RMs) for all-solid-state lithium−sulfur batteries (ASSLSBs). (a) Proposed reaction scheme of the RMs for ASSLSBs. Effective RMs solubilized in the solid polymer electrolytes (SPEs) shuttle electrons between the Li_2S particles and the current collectors. During the charging process, RM_{ox} chemically oxidizes Li_2S to polysulfides while RM_{ox} is reduced to RM_{red} (step A, chemical reaction). RM_{red} diffuses toward the current collector and is oxidized to the initial state of RM_{ox} near the current collector surface (step B, electrochemical reaction). The light blue color indicates the SPEs. (b) Schematic first charge profiles of ASSLSBs with (orange line) and without RM (blue line). A high energy barrier needs to be overcome for activating bare Li_2S. Gray: Li_2S particles; yellow: sulfur.

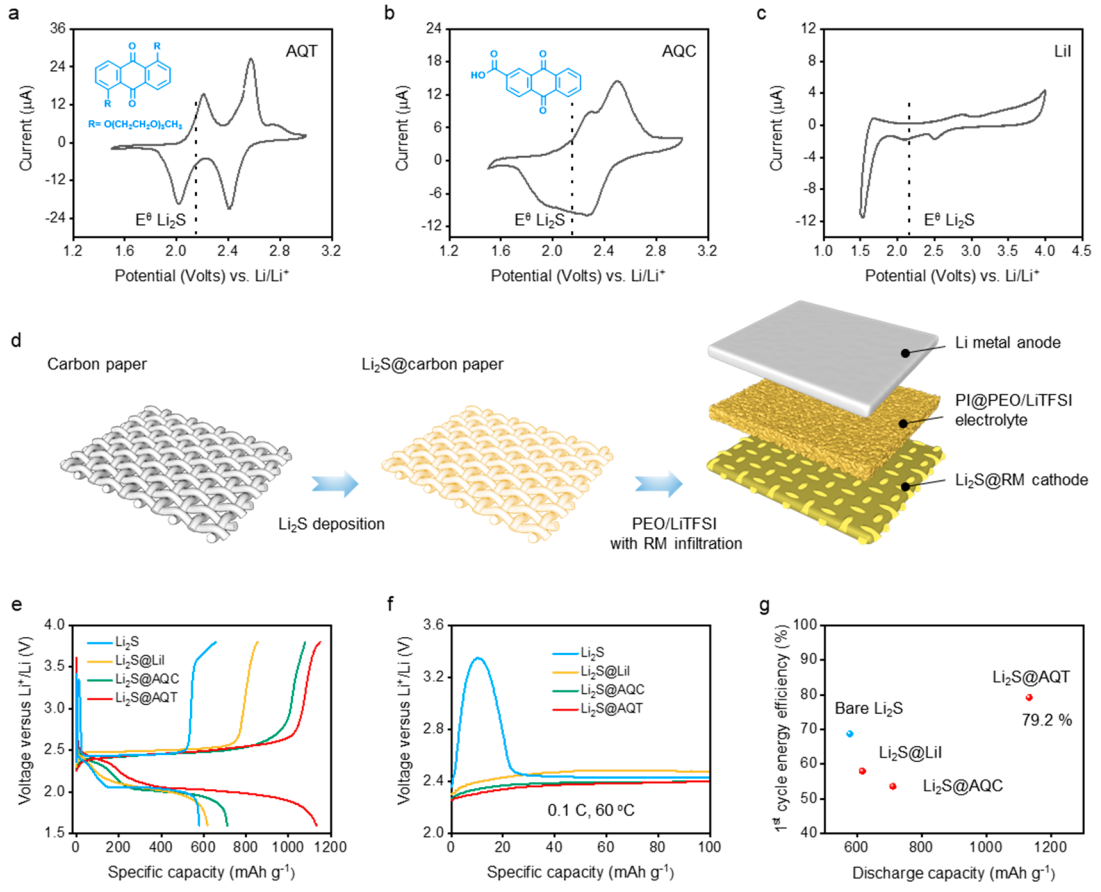

Figure 2. Design of RMs for ASSLSBs. (a−c) Cyclic voltammogram (CV) curves and chemical structure of (a) AQT, (b) AQC, and (c) LiI in PEO/LiTFSI solid polymer electrolytes (SPEs). The dotted line is the equilibrium potential of Li_2S (~2.15 V versus Li^+/Li). Scan rate, 0.1 mV s^{-1}. (d) Schematic of the fabrication process of ASSLSBs using Li_2S@RM cathodes, SPEs, and lithium metal anodes. Bare Li_2S cathodes are prepared without adding an RM additive. (e) Charge−discharge curves of Li_2S cathodes without/with RMs for the first cycle at 0.1 C. The molar ratio of Li_2S to RMs is 20:1. (f) The zoom-in charge curves of (e) to show the Li_2S activation barrier. (g) Energy efficiency and discharge capacity of Li_2S cathodes with different RMs for the first activation cycle. All the cells are operated at 60 °C.

and better scalable processing ability than inorganic electrolytes.[16,17] However, the energy density and stability achieved by polymer-based ASSLSBs to date have been far below expected due to uncontrolled active materials dissolution (lithium polysulfides, LiPSs) into SPEs[18] and sluggish lithium−sulfur (Li−S) conversion kinetics. To solve the dissolution of LiPSs in SPEs, several inorganic fillers (e.g., TiO_2,[19] Al_2O_3,[20] and some lithium-ion-conducting ceramics[21,22])-incorporated SPEs and nanoscale encapsulation of sulfur electrodes have been demonstrated.[23] Moreover, a series of lithium salts were developed to create the compact and stable solid electrolyte interphase (SEI) on the lithium metal anode to prevent the polysulfide shuttling effect.[24−27] Despite these improvements in ASSLSBs, studies on improving

https://doi.org/10.1021/jacs.1c07754
J. Am. Chem. Soc. 2021, 143, 18188−18195

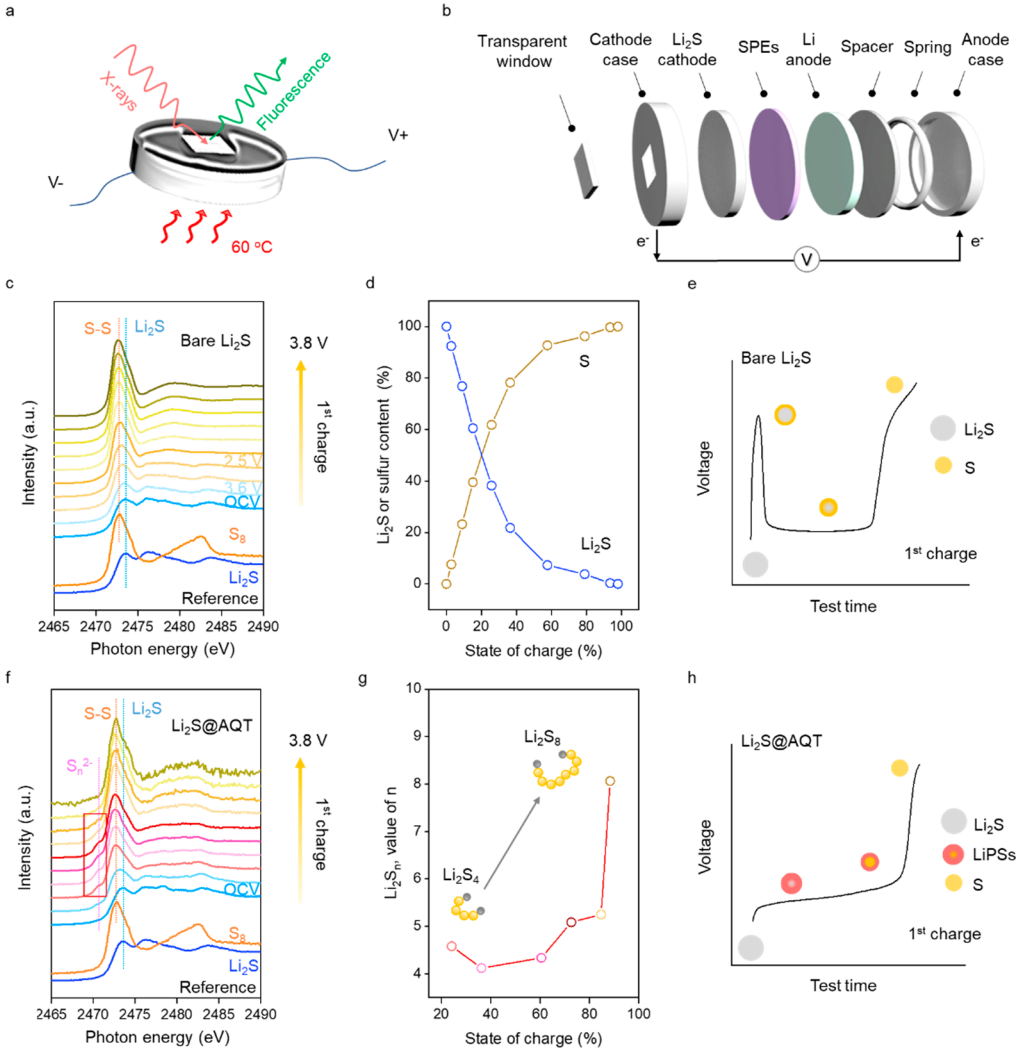

Figure 3. *Operando* X-ray absorption spectroscopy (XAS) to understand RM chemistry in ASSLSBs. (a) Schematic of the *operando* all-solid-state coin cell for X-ray spectroscopic detection and electrochemical test. (b) The cell is composed of the cathode case, Li_2S cathode, solid polymer electrolytes (SPEs), lithium metal anode, spacer, spring, and anode case. A hole (3 × 3 mm) is drilled at the cathode case and sealed by a polyester/polyethylene (PET/PE) film (63.5 μm thick). This film serves as a transparent window for X-ray beam penetration. The whole cell is heated at 60 °C for electrochemical cycles. *Operando* sulfur K-edge XAS spectra of (c) bare Li_2S cathodes and (f) Li_2S@AQT cathodes in polymer-based ASSLSBs for the first charging. XAS spectra of Li_2S (2473.5 eV) and sulfur (2472.7 eV) shown in the bottom are used as references. The pre-edge at 2470.7 eV is from the terminal sulfur of polysulfides. (d) Li_2S and sulfur contents calculated from the XAS spectra in (c) during the first charge process. The corresponding charge curve shows a high energy barrier around 4 V for Li_2S activation. Schematics for the proposed Li−S reaction mechanism in ASSLSBs, using Li_2S cathodes (e) without and (h) with AQT RM. (g) Average chain length of LiPSs versus the state of charge for Li_2S@AQT cathodes during the first charging.

sulfur reaction kinetics in solid-state electrolytes are still in their infancy. RMs with the function of electron shuttles are expected to promote sulfur species conversion and utilization. Furthermore, a deep understanding of the redox chemistry during discharge/charge in ASSLSBs is crucial to designing effective RMs.

Herein, we prove the efficacy of RMs in ASSLSBs and reveal the redox chemistry for Li_2S cathodes using *operando* X-ray absorption spectroscopy (XAS) measurements. By thoroughly evaluating the redox potential and the solubility of different RMs, soluble-type 1,5-bis(2-(2-(2-methoxyethoxy)ethoxy)-ethoxy)anthra-9,10-quinone (AQT) shows the best redox potential and redox reversibility in SPEs. As a result, the Li_2S@AQT cell shows the lowest energy barrier (average oxidation potential of 2.4 V) for the initial oxidation of Li_2S and exhibits a following discharge capacity as high as 1133 mAh g_s^{-1} at 0.1 C at 60 °C, which is nearly double that of the bare Li_2S cell (579 mAh g_s^{-1}). Using *operando* XAS, we revealed the redox chemistry of the Li−S reaction in ASSLSBs based on Li_2S cathodes. By identifying the sulfur species using the sulfur K-edge, we discovered the solid−solid Li_2S−sulfur conversion mechanism for the bare Li_2S cathode in the first charge cycle. This solid−solid conversion of the bare Li_2S cathodes results in a high energy barrier for activation (charge to ∼4 V) and low sulfur utilization. Incorporating AQT, *operando* XAS demonstrates the formation of polysulfides in the first charging and the solid−polysulfide−solid conversion mechanism in ASSLSBs based on Li_2S@AQT cathodes. Furthermore, the AQT RM reduced polarization and improved long cycling stability and Coulombic efficiency (CE, average 98.9% for 150 cycles).

https://doi.org/10.1021/jacs.1c07754
J. Am. Chem. Soc. 2021, 143, 18188−18195

RESULTS AND DISCUSSIONS

Designing Redox Mediators to Facilitate Li_2S Oxidation for ASSLSBs. The reaction mechanism of RMs in ASSLSBs is shown in Figure 1a, which is considered as a two-step process involving electrochemical and chemical reactions. During charging, oxidized RMs (RM_{ox}) chemically oxidize Li_2S to lithium polysulfides (LiPSs) while RM_{ox} is reduced to reduced RMs (RM_{red}) (step A, chemical reaction). RM_{red} in turn is electrochemically oxidized to the initial state of RM_{ox} by giving electrons to current collectors (step B). RMs shuttle electrons between the current collectors and isolated Li_2S, which would have otherwise remained inactive. The charging voltage of the cell depends on the electrochemical step (step B). Therefore, we propose that the reduced charge polarization and improved sulfur utilization for ASSLSBs can be realized by choosing an appropriate RM, as shown in Figure 1b.

Two criteria are paramount for effective RMs: (1) soluble in SPEs; (2) redox potential slightly higher than that of Li_2S. Anthraquinone (AQ) derivatives with electron-rich benzene rings are promising redox candidates. We select two typical AQ derivatives to examine their electrochemical properties in SPEs, including AQT and anthraquinone-2-carboxylic acid (AQC). Lithium iodide (LiI), a typical redox mediator in liquid electrolytes,[9,28,29] is compared in SPEs as a reference. RMs are first mixed with poly(ethylene oxide) (PEO)/lithium bis(trifluoromethanesulfonyl)imide (LiTFSI) electrolytes in acetonitrile solution (mixtures shown in Supplementary Figure 1) and then drop-casted on the carbon paper as the electrodes. Figure 2a−c show cyclic voltammogram (CV) curves of the RM electrodes versus lithium metal in PEO/LiTFSI SPEs. Compared with LiI and AQC, AQT showed the most favorable redox potentials, matching that of Li_2S oxidation and best redox reversibility.

Li_2S cathodes with AQT (Li_2S@AQT) are fabricated by infiltrating PEO/LiTFSI solution with RMs into the Li_2S-coated carbon paper (Figure 2d). The Li_2S cathode without adding RMs is used as a control. The molar ratio of Li_2S to RM is 20:1. ASSLSBs are fabricated with Li_2S cathodes, PEO/LiTFSI electrolytes, and lithium anodes. Figure 2e presents the first charge−discharge profiles of Li_2S cells with/without RMs at 0.1 C at 60 °C. The bare Li_2S cell shows a high energy barrier of 3.4 V and low-energy efficiency (less than 70%) at the initial activation cycle, because of the large charge transfer resistance from the direct oxidation of Li_2S.[30,31] After incorporating the RMs, the activation barrier of Li_2S decreases below 2.5 V (Figure 2f). Compared with AQC and LiI, Li_2S@AQT cells represent the lowest average oxidation potential of 2.4 V and the highest energy efficiency of 79.2% for the first cycle (Figure 2g). This agrees well with our design rationales in Figure 1. A specific capacity of 1133 mAh g_s^{-1} at 0.1 C at the first cycle is realized by the Li_2S@AQT cell, which nearly doubles that of the bare Li_2S cell (579 mAh g_s^{-1}) (Figure 2g). The reversible capacity and CE further increase when the AQT concentration increases (Supplementary Figure 2). Since adding AQT increases the mass of inactive materials to some extent, we choose the molar ratio of 20:1 in the following study. To evaluate the stability of polymer electrolytes with AQT toward lithium metal anodes, we performed the Aurbach test in Cu|Li cells (Supplementary Figure 3). The CE of Cu|Li cells with AQT is 93%, while the CE for the bare PEO/LiTFSI electrolytes is only 89%. Lithium fluoride (LiF) and lithium oxide (Li_2O) are detected at the SEI of deposited lithium in PEO/LiTFSI electrolytes with AQT (Supplementary Figure 4). This interphase layer helps to stabilize the electrolyte/electrode interface.

Understanding Redox Chemistry in ASSLSBs. To further understand the roles of effective RMs, proper *operando* characterization techniques are required. *Operando* XAS[32−34] can directly visualize the chemical-state evolution of the working electrode in real time, allowing us to explore the RM behavior and uncover the sulfur speciation during battery operation for ASSLSBs. Here, we for the first time perform the *operando* XAS measurements for Li_2S electrodes in polymer-based ASSLSBs. Figure 3a and b show the designed *operando* coin cell, which can simultaneously perform electrochemical cycle and X-ray spectroscopic measurement. To exclude the contribution of sulfur absorption from LiTFSI, we used poly(ethylene oxide)/lithium perchlorate (PEO/$LiClO_4$) as a model system to study the underlying mechanism. Commercial Li_2S particles (average diameter of 15 μm, SEM image shown in Supplementary Figure 5) mixed with PEO/$LiClO_4$ electrolytes are deposited on the carbon paper as the cathodes. A PEO/$LiClO_4$ (EO/Li^+, 10:1)-infiltrated porous polyethylene film serves as the SPE layer, and lithium metal is the anode. A hole (3 × 3 mm) is drilled at the cathode case and sealed by a transparent polyester/polyethylene (PET/PE) film (63.5 μm thick) for X-ray beam penetration. The cell was charged to a cutoff voltage of 3.8 V at 10 μA cm^{-2} at 60 °C. Figure 3c shows the *operando* XAS of the Li_2S−Li cell during the first cycle. At the open-circuit voltage (OCV), the XAS spectrum for Li_2S cathodes shows a feature at 2473.5 eV, indicating pure Li_2S at the pristine state.[34−36] As the charging process proceeds, an additional peak at 2472.7 eV, assigned to the S 1s to 3p transition of elemental sulfur,[34−36] appears. The intensity of the sulfur peak increases with continued delithiation. Meanwhile, no extra pre-edge feature corresponding to the terminal sulfur of polysulfides[35,36] at 2470.7 eV is observed, indicating no detectable polysulfide formation. The overpotential drop after the initial activation process is likely due to slight polysulfide formation from the chemical reaction between Li_2S and sulfur. However, the amount of formed polysulfides is lower than the detect limitation of XAS. To further quantify the content change of Li_2S and sulfur during the first charging process, the two-phase fitting for the *operando* XAS spectra[34] was conducted. The content of Li_2S decreases monotonously as the charge proceeds, while that of sulfur is increased (Figure 3d). Therefore, we propose that Li_2S is gradually consumed and converted to sulfur though a solid−solid reaction in the first charge process (Figure 3e), showing the sluggish Li_2S oxidation in ASSLSBs.

To understand the redox chemistry after incorporating AQT RM, we conduct *operando* sulfur K-edge XAS measurements for Li_2S@AQT electrodes. The *operando* XAS results with reference samples are shown in Figure 3f. The feature of elemental sulfur at 2472.7 eV shows a gradual increase, which indicates the transformation from Li_2S to sulfur during the charging process. Particularly, typical features of LiPSs (2470.7 eV) are observed from the XAS spectra in the red rectangle in Figure 3f, while they are not observed for bare Li_2S cathodes during the whole first charge process. Moreover, we also conduct the *operando* XAS measurement to reveal the working mechanism of AQT in the PEO/LiTFSI electrolyte (Supplementary Figure 6). The polysulfide formation is also observed

https://doi.org/10.1021/jacs.1c07754
J. Am. Chem. Soc. 2021, 143, 18188−18195

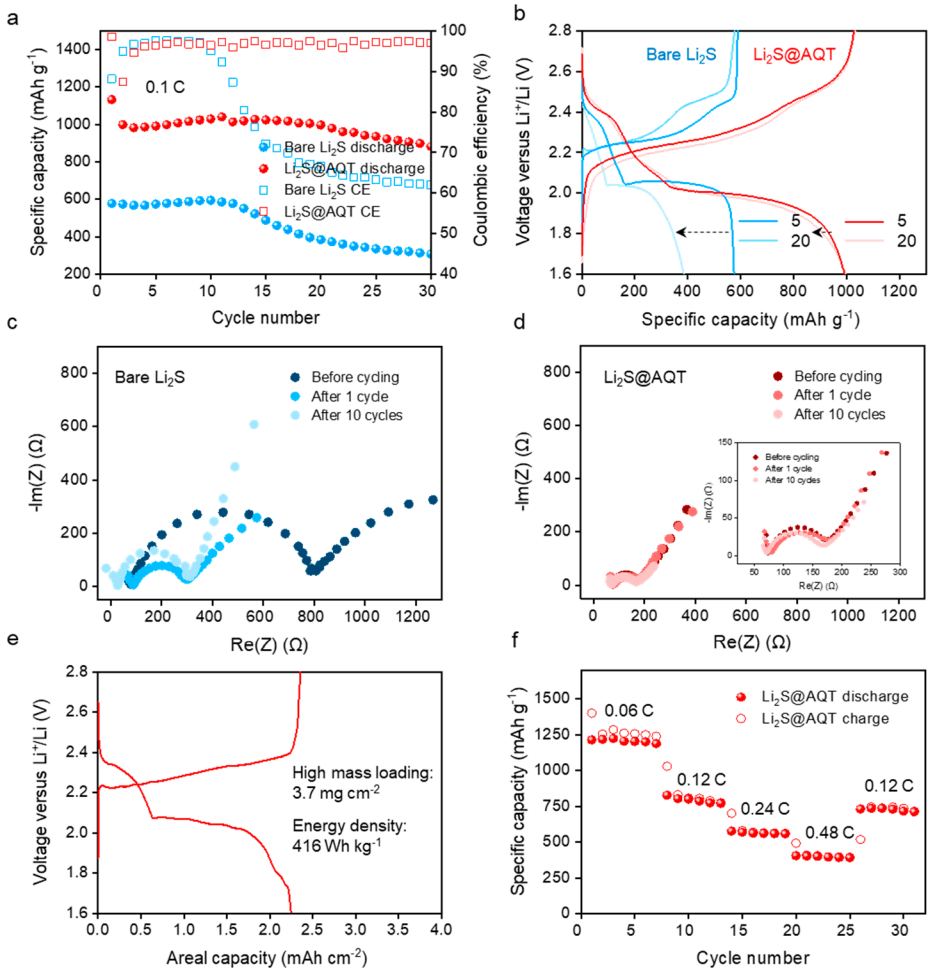

Figure 4. Electrochemical performance of Li_2S cathodes without/with AQT RM in ASSLSBs. (a) Cycling performance and Coulombic efficiency of Li_2S cathodes without/with AQT at 0.1 C for 30 cycles. (b) Typical charge−discharge voltage profiles of Li_2S cathodes without/with AQT at the 5th cycle and the 20th cycle at 0.1 C. Nyquist plots of (c) the bare Li_2S cell and (d) the Li_2S@AQT cell before and after different cycles. Inset in Figure 4d shows the zoom-in Nyquist plot for the Li_2S@AQT cell. (e) Voltage profile at the second cycle of the Li_2S@AQT cell with a Li_2S mass loading (3.7 mg cm^{-2}) at 0.25 mA cm^{-2} at 60 °C. (f) Specific capacity of the Li_2S@AQT cell cycled from 0.06 to 0.48 C. All cells are operated at 60 °C.

during the first charging of the AQT-incorporated Li−S cell. A strong LiTFSI peak is shown at 2480.3 eV for all the spectra.

We further calculate the average chain length of LiPSs at different charge stages based on the area ratio of main-edge peaks to pre-edge peaks.[33,35] Figure 3g shows the average chain length of LiPSs (n) during the charging. At the beginning of charging, the value of n is around 4 and then significantly increases to 8 as the electrochemical reaction proceeds. At the end of the charging, the pre-edge feature of LiPSs disappears while the main-edge feature of the elemental sulfur (2472.7 eV) becomes more prominent.

These results indicate Li_2S cathodes with AQT undergo a different Li−S reaction mechanism with bare Li_2S for the activation cycle, as proposed in Figure 3e and h. AQT has a higher redox potential (~2.4 V) than Li_2S (~2.1 V), which promotes Li_2S oxidation in SPEs by chemically oxidizing Li_2S to LiPSs. The reduced AQT diffuses to current collectors and then is electrochemically reoxidized. The redox activity of AQT is further verified by the CV test (Supplementary Figure 7). It shows reduction peaks from both AQT and Li_2S in the Li_2S@AQT cell, while only reduction peaks from Li_2S are in the pristine Li_2S cell. The oxidation peak of reduced AQT is overlapped with the broadened oxidation peak of Li_2S. The reaction cycle proceeds until all Li_2S are fully oxidized and activated. As a result, the charge voltage reflects the redox potential of AQT, which is much lower than the potential of bare Li_2S activation. It is consistent with the electrochemical results in Figure 2e.

After the first activation cycle, we collected the XAS spectra at several typical charge voltages during the following charge process (Supplementary Figure 8). The two-phase fitting method[34] was used to calculate the contents of Li_2S and sulfur at the fully charged state. For bare Li_2S cathodes, the ratio of Li_2S to sulfur is 59/41, which indicates nearly one-half of Li_2S does not convert to sulfur, thus showing a much lower practical capacity than that of the theoretical prediction. On the contrary, AQT can shuttle electrons between the current collectors and isolated Li_2S, which would have otherwise remained inactive. Therefore, Li_2S cathodes with AQT show an improved Li_2S utilization, with a ratio of 18/82 for Li_2S to sulfur at a fully charged state. Similar results were obtained by XPS measurements of *ex-situ* coin cells after cycling (Supplementary Figure 9).

Electrochemical Performance of Li_2S Cathodes with AQT in ASSLSBs. We further prove the efficacy of AQT beyond the first activation cycle in ASSLSBs by testing the

https://doi.org/10.1021/jacs.1c07754
J. Am. Chem. Soc. 2021, 143, 18188−18195

cycling performance of Li_2S cathodes without/with AQT. As-assembled cells are first charged to 3.8 V for Li_2S activation, then cycled from 1.6 to 2.8 V at 0.1 C. Incorporating AQT RM significantly improves the cycling stability of ASSLSBs (Figure 4a and b). The bare Li_2S cell shows the fast capacity decay (from 579 mAh g_s^{-1} to 384 mAh g_s^{-1}) within 20 cycles at 0.1 C with a lower average Coulombic efficiency of 85%. In contrast, the Li_2S@AQT cell shows a stabilized capacity, retained at 997 mA h g_s^{-1} after 20 cycles, and sustains more than 150 cycles with an average CE of 98.9% (Figure 4a and Supplementary Figure 10). It outperforms most previously reported PEO-based ASSLSBs (Supplementary Table 1). The capacity decay is mainly due to increased cell polarization during cycling. No optimized processing is made for the commercial Li_2S (ball milling or encapsulation).

The enhanced cycling performance of Li_2S@AQT cells is attributed to preventing the formation of the thick sulfur/Li_2S passivation layer and decreasing the amount of soluble sulfur species in the SPEs, which are further verified by *operando* impedance and optical cell studies (Figure 4c,d and Supplementary Figure 11). Before cycling, the impedance spectrum of the bare Li_2S cell shows a larger semicircle than that of the Li_2S@AQT cell in the high-frequency region, indicating higher charge-transfer resistance in the bare Li_2S cell (Figure 4c and d). After cycling, the impedance of the Li_2S@AQT cell remains low and stable over 10 cycles. In contrast, the bare Li_2S cell exhibits a high and increased impedance. It is noted that the decreased impedance after the first cycle for bare Li_2S cathodes results from the enhanced contact between cathodes and SPEs. Moreover, *operando* optical cell measurement (Supplementary Figure 11) indicates adding AQT decreases the dissolved sulfur species in the SPEs, owing to promoted reaction kinetics and the strong binding of Li_2S/Li_2S_x species to AQT.[9] After incorporating AQT, polysulfides prefer to stay on the cathode side and are rapidly oxidized/reduced during charging/discharging. Additionally, the Li_2S@AQT cell with a high mass loading of Li_2S (3.7 mg cm^{-2}) was assembled and tested at 60 °C. The as-prepared Li_2S@AQT cell shows a high areal capacity of 2.3 mA h cm^{-2} (Figure 4e) and a high cell-level energy density (416 Wh kg^{-1}) based on the mass of the Li_2S cathode (excluding the current collector), the PEO-based electrolyte with RMs, and the lithium metal anode. Supplementary Figure 12 displays the cycling performance of high-loading ASSLSBs with RMs at 250 mA cm^{-2}. The cycling exhibits a slight capacity fading for a few equilibrium cycles and remains stable with a capacity of 640 mA h g^{-1} after 15 cycles.

Finally, Li_2S@AQT cells were cycled at different C-rates to investigate the rate performance. As shown in Figure 4f, Li_2S@AQT cells achieve a discharge capacity of 1214, 827, 577, and 406 mAh g_s^{-1} at 0.06, 0.12, 0.24, and 0.48 C, respectively. It outperforms most previously reported ASSLSBs.[24,25,37,38] All the above results show that AQT enables promoted reaction kinetics and stability to achieve high-performance ASSLSBs.

CONCLUSIONS

In summary, we have successfully proved that RMs are effective in all-solid-state batteries. An anthraquinone-based redox center with a suitable redox potential, good stability, and high solubility in the SPEs was rationally designed to facilitate Li_2S oxidation. Using *operando* sulfur K-edge X-ray absorption spectroscopy, we directly tracked the sulfur speciation and revealed the redox chemistry for Li_2S cathodes in ASSLSBs for the first time. Li_2S cathodes with AQT RMs deliver a discharge capacity as high as 1133 mAh g_s^{-1}. The Li_2S@AQT cell demonstrates superior cycling stability (average Coulombic efficiency 98.9% for 150 cycles) and rate capability owing to the effective AQT-enhanced Li−S reaction kinetics. This study opens a new avenue for developing next-generation solid-state batteries with high energy density, high safety, and long cycle life.

METHODS

Preparation of Li_2S Cathodes. The 1 M Li_2S colloidal solution is drop-casted onto the free-standing carbon paper (Fuel Cell Store, AvCarb P50). Then, Li_2S@RM cathodes are fabricated by infiltrated PEO (MW = 300 000)/LiTFSI solution (EO to Li is 10:1) with RMs into the Li_2S-coated carbon paper and dried at 80 °C. The molar ratio of Li_2S to RMs is 20:1. Bare Li_2S cathodes are synthesized following a process similar to that of Li_2S@RM except without the addition of RMs. The mass loading of Li_2S is 0.2−0.7 mg cm^{-2}. All the procedures were conducted in an argon-filled glovebox.

***Operando* XAS study.** *Operando* coin cells were adapted from the type 2032 coin cells. A hole (3 × 3 mm) is drilled at the cathode case and sealed by a PET/PE film (63.5 μm thick) for X-ray beam penetration. The working electrode is bare Li_2S or Li_2S@AQT. The counter electrode is lithium metal. PEO/$LiClO_4$ acted as the electrolyte to connect the two electrodes. The *operando* electrochemical reaction is performed with a Bio-Logic SP-50, which simultaneously collects the sulfur K-edge XAS spectra for working electrodes. The *operando* cell is galvanostatically charged to 3.8 V at 10 μA cm^{-2} and then discharged to 1.6 V. Sulfur K-edge X-ray absorption spectroscopy measurements are performed at beamline 4-3 at the Stanford Synchrotron Radiation Light source of SLAC National Accelerator Laboratory. Data are calibrated, normalized, and further analyzed using Athena software.

Electrochemical Performance Measurements. ASSLSBs are assembled using Li_2S cathodes, PEO-based electrolytes (10−20 μm), and lithium metal anodes (∼50 μm) in an argon-filled glovebox. As-prepared coin cells (type 2032) are tested with a Land battery testing system. The first charge cycle is cut off at 3.8 V to fully activate the Li_2S electrode. The following cycles are between 1.6 and 2.8 V. CV and electrochemical impedance spectroscopy (EIS) measurements are performed using a Bio-Logic VMP3. Temperature-controlled experiments are performed in an environmental chamber (BTU-133, ESPEC North America).

ASSOCIATED CONTENT

Supporting Information

The Supporting Information is available free of charge at https://pubs.acs.org/doi/10.1021/jacs.1c07754.

Experimental details and methods, including redox mediator synthesis, polymer electrolyte preparation, electrochemical performance measurements, and energy density calculation; tables and figures for electrochemical testing and material characterization (PDF)

AUTHOR INFORMATION

Corresponding Author

Yi Cui − *Department of Materials Science and Engineering, Stanford University, Stanford, California 94305, United States; Stanford Institute for Materials and Energy Sciences, SLAC National Accelerator Laboratory, Menlo Park, California 94025, United States;* orcid.org/0000-0002-6103-6352; Email: yicui@stanford.edu

Authors

Xin Gao − *Department of Materials Science and Engineering, Stanford University, Stanford, California 94305, United States;* orcid.org/0000-0001-5360-0796

Xueli Zheng − *Department of Materials Science and Engineering, Stanford University, Stanford, California 94305, United States;* orcid.org/0000-0002-6800-2649

Yuchi Tsao − *Department of Chemistry, Stanford University, Stanford, California 94305, United States*

Pu Zhang − *Department of Materials Science and Engineering, Stanford University, Stanford, California 94305, United States*

Xin Xiao − *Department of Materials Science and Engineering, Stanford University, Stanford, California 94305, United States;* orcid.org/0000-0003-1098-9484

Yusheng Ye − *Department of Materials Science and Engineering, Stanford University, Stanford, California 94305, United States;* orcid.org/0000-0001-9832-2478

Jun Li − *Department of Materials Science and Engineering, Stanford University, Stanford, California 94305, United States; Department of Chemistry, Stanford University, Stanford, California 94305, United States;* orcid.org/0000-0003-4660-1234

Yufei Yang − *Department of Materials Science and Engineering, Stanford University, Stanford, California 94305, United States*

Rong Xu − *Department of Materials Science and Engineering, Stanford University, Stanford, California 94305, United States*

Zhenan Bao − *Department of Chemical Engineering, Stanford University, Stanford, California 94305, United States;* orcid.org/0000-0002-0972-1715

Complete contact information is available at: https://pubs.acs.org/10.1021/jacs.1c07754

Notes

The authors declare no competing financial interest.

■ ACKNOWLEDGMENTS

Y.C. and Z. B. acknowledge the support from the Assistant Secretary for Energy Efficiency and Renewable Energy, Office of Vehicle Technologies, of the U.S. Department of Energy under the Battery Materials Research (BMR) Program and the Battery500 Consortium program. We thank Erik Nelson and Matthew Latimer for their assistance at BL 4-3 at the Stanford Synchrotron Radiation Light source of SLAC National Accelerator Laboratory. Use of the Stanford Synchrotron Radiation Lightsource, SLAC National Accelerator Laboratory, is supported by the U.S. Department of Energy, Office of Science, Office of Basic Energy Sciences under Contract No. DE-AC02-76SF00515. X.G. acknowledges Dr. Fang Liu for the discussions.

■ REFERENCES

(1) Tamirat, A. G.; Guan, X.; Liu, J.; Luo, J.; Xia, Y. Redox mediators as charge agents for changing electrochemical reactions. *Chem. Soc. Rev.* **2020**, *49* (20), 7454−7478.

(2) Kang, X. Nonaqueous Liquid Electrolytes for Lithium-Based Rechargeable Batteries. *Chem. Rev.* **2004**, *104* (10), 4303−4418.

(3) Zhang, L.; Zhang, Z.; Wu, H.; Amine, K. Novel redox shuttle additive for high-voltage cathode materials. *Energy Environ. Sci.* **2011**, *4* (8), 2858−2862.

(4) Lee, K. T. Roles of Surface Chemistry on Safety and Electrochemistry in Lithium Ion Batteries. *Acc. Chem. Res.* **2013**, *46* (5), 1161−1170.

(5) Bruce, P. G.; Freunberger, S. A.; Hardwick, L. J.; Tarascon, J. M. Li-O_2 and Li-S batteries with high energy storage. *Nat. Mater.* **2012**, *11* (1), 19−29.

(6) Lim, H.-D.; Lee, B.; Zheng, Y.; Hong, J.; Kim, J.; Gwon, H.; Ko, Y.; Lee, M.; Cho, K.; Kang, K. Rational design of redox mediators for advanced Li-O_2 batteries. *Nat. Energy* **2016**, *1* (6), 1−9.

(7) Park, J. B.; Lee, S. H.; Jung, H. G.; Aurbach, D.; Sun, Y. K. Redox Mediators for Li-O_2 Batteries: Status and Perspectives. *Adv. Mater.* **2018**, *30* (1), 1704162.

(8) Leverick, G.; Tułodziecki, M.; Tatara, R.; Bardé, F.; Shao-Horn, Y. Solvent-Dependent Oxidizing Power of LiI Redox Couples for Li-O_2 Batteries. *Joule* **2019**, *3* (4), 1106−1126.

(9) Tsao, Y.; Lee, M.; Miller, E. C.; Gao, G.; Park, J.; Chen, S.; Katsumata, T.; Tran, H.; Wang, L.-W.; Toney, M. F.; Cui, Y.; Bao, Z. Designing a Quinone-Based Redox Mediator to Facilitate Li_2S Oxidation in Li-S Batteries. *Joule* **2019**, *3* (3), 872−884.

(10) Peng, H. J.; Zhang, G.; Chen, X.; Zhang, Z. W.; Xu, W. T.; Huang, J. Q.; Zhang, Q. Enhanced Electrochemical Kinetics on Conductive Polar Mediators for Lithium-Sulfur Batteries. *Angew. Chem., Int. Ed.* **2016**, *55* (42), 12990−12995.

(11) Li, G.; Wang, X.; Seo, M. H.; Li, M.; Ma, L.; Yuan, Y.; Wu, T.; Yu, A.; Wang, S.; Lu, J.; Chen, Z. Chemisorption of polysulfides through redox reactions with organic molecules for lithium-sulfur batteries. *Nat. Commun.* **2018**, *9* (1), 1−10.

(12) Manthiram, A.; Chung, S. H.; Zu, C. Lithium-sulfur batteries: progress and prospects. *Adv. Mater.* **2015**, *27* (12), 1980−2006.

(13) Li, S.; Zhang, W.; Zheng, J.; Lv, M.; Song, H.; Du, L. Inhibition of Polysulfide Shuttles in Li-S Batteries: Modified Separators and Solid-State Electrolytes. *Adv. Energy Mater.* **2021**, *11* (2), 2000779.

(14) Ji, X.; Lee, K. T.; Nazar, L. F. A highly ordered nanostructured carbon-sulphur cathode for lithium-sulphur batteries. *Nat. Mater.* **2009**, *8* (6), 500−506.

(15) Manthiram, A.; Yu, X.; Wang, S. Lithium battery chemistries enabled by solid-state electrolytes. *Nat. Rev. Mater.* **2017**, *2* (4), 1−16.

(16) Zhao, Q.; Stalin, S.; Zhao, C.-Z.; Archer, L. A. Designing solid-state electrolytes for safe, energy-dense batteries. *Nat. Rev. Mater.* **2020**, *5* (3), 229−252.

(17) Li, Z.; Zhang, H.; Sun, X.; Yang, Y. Mitigating Interfacial Instability in Polymer Electrolyte-Based Solid-State Lithium Metal Batteries with 4 V Cathodes. *ACS Energy Lett.* **2020**, *5* (10), 3244−3253.

(18) Song, Y.-X.; Shi, Y.; Wan, J.; Lang, S.-Y.; Hu, X.-C.; Yan, H.-J.; Liu, B.; Guo, Y.-G.; Wen, R.; Wan, L.-J. Direct tracking of the polysulfide shuttling and interfacial evolution in all-solid-state lithium-sulfur batteries: a degradation mechanism study. *Energy Environ. Sci.* **2019**, *12* (8), 2496−2506.

(19) Croce, F. Nanocomposite polymer electrolytes for lithium batteries. *Nature* **1998**, *394* (6692), 456−458.

(20) Judez, X.; Zhang, H.; Li, C.; Eshetu, G. G.; Zhang, Y.; Gonzalez-Marcos, J. A.; Armand, M.; Rodriguez-Martinez, L. M. Polymer-Rich Composite Electrolytes for All-Solid-State Li-S Cells. *J. Phys. Chem. Lett.* **2017**, *8* (15), 3473−3477.

(21) Tao, X.; Liu, Y.; Liu, W.; Zhou, G.; Zhao, J.; Lin, D.; Zu, C.; Sheng, O.; Zhang, W.; Lee, H. W.; Cui, Y. Solid-State Lithium-Sulfur Batteries Operated at 37 degrees C with Composites of Nano-structured $Li_7La_3Zr_2O_{12}$/Carbon Foam and Polymer. *Nano Lett.* **2017**, *17* (5), 2967−2972.

(22) Zhang, T.; He, W.; Zhang, W.; Wang, T.; Li, P.; Sun, Z.; Yu, X. Designing composite solid-state electrolytes for high performance lithium ion or lithium metal batteries. *Chem. Sci.* **2020**, *11* (33), 8686−8707.

(23) Gao, X.; Zheng, X.; Wang, J.; Zhang, Z.; Xiao, X.; Wan, J.; Ye, Y.; Chou, L. Y.; Lee, H. K.; Wang, J.; Vila, R. A.; Yang, Y.; Zhang, P.; Wang, L. W.; Cui, Y. Incorporating the Nanoscale Encapsulation Concept from Liquid Electrolytes into Solid-State Lithium-Sulfur Batteries. *Nano Lett.* **2020**, *20* (7), 5496−5503.

(24) Zhang, H.; Oteo, U.; Judez, X.; Eshetu, G. G.; Martinez-Ibañez, M.; Carrasco, J.; Li, C.; Armand, M. Designer Anion Enabling Solid-State Lithium-Sulfur Batteries. *Joule* **2019**, *3* (7), 1689−1702.
(25) Judez, X.; Zhang, H.; Li, C.; Gonzalez-Marcos, J. A.; Zhou, Z.; Armand, M.; Rodriguez-Martinez, L. M. Lithium Bis(fluorosulfonyl)-imide/Poly(ethylene oxide) Polymer Electrolyte for All Solid-State Li-S Cell. *J. Phys. Chem. Lett.* **2017**, *8* (9), 1956−1960.
(26) Eshetu, G. G.; Judez, X.; Li, C.; Martinez-Ibanez, M.; Gracia, I.; Bondarchuk, O.; Carrasco, J.; Rodriguez-Martinez, L. M.; Zhang, H.; Armand, M. Ultrahigh Performance All Solid-State Lithium Sulfur Batteries: Salt Anion's Chemistry-Induced Anomalous Synergistic Effect. *J. Am. Chem. Soc.* **2018**, *140* (31), 9921−9933.
(27) Eshetu, G. G.; Judez, X.; Li, C.; Bondarchuk, O.; Rodriguez-Martinez, L. M.; Zhang, H.; Armand, M. Lithium Azide as an Electrolyte Additive for All-Solid-State Lithium-Sulfur Batteries. *Angew. Chem., Int. Ed.* **2017**, *56* (48), 15368−15372.
(28) Wu, F.; Lee, J. T.; Nitta, N.; Kim, H.; Borodin, O.; Yushin, G. Lithium iodide as a promising electrolyte additive for lithium-sulfur batteries: mechanisms of performance enhancement. *Adv. Mater.* **2015**, *27* (1), 101−108.
(29) Meini, S.; Elazari, R.; Rosenman, A.; Garsuch, A.; Aurbach, D. The Use of Redox Mediators for Enhancing Utilization of Li_2S Cathodes for Advanced Li-S Battery Systems. *J. Phys. Chem. Lett.* **2014**, *5* (5), 915−918.
(30) Ye, H.; Li, M.; Liu, T.; Li, Y.; Lu, J. Activating Li_2S as the Lithium-Containing Cathode in Lithium-Sulfur Batteries. *ACS Energy Lett.* **2020**, *5* (7), 2234−2245.
(31) Yang, Y.; Zheng, G.; Misra, S.; Nelson, J.; Toney, M. F.; Cui, Y. High-capacity micrometer-sized Li2S particles as cathode materials for advanced rechargeable lithium-ion batteries. *J. Am. Chem. Soc.* **2012**, *134* (37), 15387−15394.
(32) Cuisinier, M.; Cabelguen, P.-E.; Evers, S.; He, G.; Kolbeck, M.; Garsuch, A.; Bolin, T.; Balasubramanian, M.; Nazar, L. F. Sulfur Speciation in Li-S Batteries Determined by Operando X-ray Absorption Spectroscopy. *J. Phys. Chem. Lett.* **2013**, *4* (19), 3227−3232.
(33) Wujcik, K. H. In Situ X-ray Absorption Spectroscopy Studies of Discharge Reactions in a Thick Cathode of a Lithium Sulfur Battery. *J. Electrochem. Soc.* **2017**, *164* (2), A18−A27.
(34) Zhang, L.; Sun, D.; Feng, J.; Cairns, E. J.; Guo, J. Revealing the Electrochemical Charging Mechanism of Nanosized Li2S by in Situ and Operando X-ray Absorption Spectroscopy. *Nano Lett.* **2017**, *17* (8), 5084−5091.
(35) Pascal, T. A.; Wujcik, K. H.; Velasco-Velez, J.; Wu, C.; Teran, A. A.; Kapilashrami, M.; Cabana, J.; Guo, J.; Salmeron, M.; Balsara, N.; Prendergast, D. X-ray Absorption Spectra of Dissolved Polysulfides in Lithium-Sulfur Batteries from First-Principles. *J. Phys. Chem. Lett.* **2014**, *5* (9), 1547−1551.
(36) Li, X.; Banis, M.; Lushington, A.; Yang, X.; Sun, Q.; Zhao, Y.; Liu, C.; Li, Q.; Wang, B.; Xiao, W.; Wang, C.; Li, M.; Liang, J.; Li, R.; Hu, Y.; Goncharova, L.; Zhang, H.; Sham, T. K.; Sun, X. A high-energy sulfur cathode in carbonate electrolyte by eliminating polysulfides via solid-phase lithium-sulfur transformation. *Nat. Commun.* **2018**, *9* (1), 1−10.
(37) Yang, X.; Luo, J.; Sun, X. Towards high-performance solid-state Li-S batteries: from fundamental understanding to engineering design. *Chem. Soc. Rev.* **2020**, *49* (7), 2140−2195.
(38) Ma, Q.; Qi, X.; Tong, B.; Zheng, Y.; Feng, W.; Nie, J.; Hu, Y. S.; Li, H.; Huang, X.; Chen, L.; Zhou, Z. Novel Li[(CF_3SO_2)(n-$C_4F_9SO_2$)N]-Based Polymer Electrolytes for Solid-State Lithium Batteries with Superior Electrochemical Performance. *ACS Appl. Mater. Interfaces* **2016**, *8* (43), 29705−29712.

https://doi.org/10.1021/jacs.1c07754
J. Am. Chem. Soc. 2021, 143, 18188−18195